

# Structural criterion for the onset of rigidity in a colloidal gel

C. S. Dias,<sup>1,2,\*</sup> J. C. Neves,<sup>1,2,†</sup> M. M. Telo da Gama,<sup>1,2,‡</sup> E. Del Gado,<sup>3,§</sup> and N. A. M. Araújo<sup>1,2,¶</sup>

<sup>1</sup>*Centro de Física Teórica e Computacional, Faculdade de Ciências,  
Universidade de Lisboa, 1749-016 Lisboa, Portugal*

<sup>2</sup>*Departamento de Física, Faculdade de Ciências,  
Universidade de Lisboa, 1749-016 Lisboa, Portugal*

<sup>3</sup>*Department of Physics, Institute for Soft Matter Synthesis and Metrology,  
Georgetown University, Washington, D.C. 20057, USA*

Identifying the necessary conditions for the onset of rigidity in a gel remains a challenge. It has been suggested that local particle coordination could be used to establish such conditions, but rigid gels occur for various coordination numbers. Combining simulations, oscillatory rheology, and a percolation analysis, for particles where the valence can be controlled, we find that the onset of rigidity coincides with the percolation of particles with three or more bonds, which arises after the connectivity percolation. We show that the rigidity results from an interplay of bonding and non-bonding interactions, providing insight into low-valence colloidal gel rigidity.

Colloidal gels are non-equilibrium structures sustained by a percolating network of long-living bonds between the particles in solution [1–5]. They exhibit unique structural [6–9], dynamical [10–12], and mechanical [13–15] properties, which have motivated an intensive search for strategies to design them. This effort is relevant to a range of industrial applications, from food to cosmetics, and from energy materials to biotechnology and construction [16–20]. Recently, one focus has been on the design of low density gels and in the control of their local structures [21–33]. This may be achieved using, for example, vitrimetric materials or patchy particles, which limit the valence of the particles and the directionality of the bonds [34–37], helping to design the gel structures.

The key property of colloidal gels is their capacity to bear load without deforming permanently. However, the necessary condition for a gel to be rigid is still under debate [38]. This question is even more critical in the design of low-density gels, where the reduced number of bonds per particle may compromise the mechanical stability. During gelation, bonds are established between pairs of particles until a percolating network of bonds emerges at a critical fraction of bonds per particle [2–5, 39]. At the onset of this connectivity percolation, the gels are floppy and fragile [40–42]. As more bonds are formed, a rigid elastic network emerges at a rigidity percolation transition [13, 43]. The necessary conditions for the rigidity percolation are unclear, since it is difficult to identify which subset of the visible structure is responsible for the stress transmission [13]. In 2D the onset of rigidity is identified directly from the bond network with the pebble game devised for rigidity percolation [44–46], but in 3D the criteria remain elusive. Several local and global geometrical criteria have been proposed, such as a minimum average coordination number [41] or the existence of a directed percolating path [40], but a recently correlated rigidity percolation framework highlights the non-local nature of the emergence of rigidity, casting doubts on the previously proposed criteria [13].

Experiments combining confocal microscopy with microrheology in colloidal gels resulting from depletion forces suggest that the onset of rigidity coincides with the percolation of particles with at least six neighbors [47], in line with a local Maxwell rigidity criterion for isostaticity [48]. However recent experiments and simulations have clarified that this local criterion does not provide the necessary conditions for gel rigidity [38]. While attractive depletion forces are isotropic and pairs of bonded particles are free to rotate relative to each other [48], rotational degrees of freedom can be hindered by molecules grafted on the particle surfaces [49–51] and, quite generally, by more complex surface interactions [12, 52, 53].

Experimentally, the count of neighbors is based on the number of particles within a certain *bonding* distance, which becomes problematic when different types of interactions are present. Here, we perform numerical simulations for gels consisting of particles with fixed valence, allowing us to distinguish bonds from contacts. We show that this difference is not a mere detail. For gels of limited valence, rigidity does emerge from the interplay of bonds and repulsive (contact) interactions. We find that the onset of rigidity coincides with the emergence of a spanning aggregate of particles with at least three bonds for any value of the valence, including the isotropic continuum limit. This poses challenges for the development of algorithms like the *pebble game* which aim at identifying the onset of rigidity by decomposing the network into local features [44].

Colloidal particles with limited valence spontaneously form gels of very-low density [54–58], with the focus of most theoretical and numerical works being the connectivity percolation [21, 59–62]. However, for most practical applications, it is critical that the gel is rigid. From the findings reported here, it is clear that the relevant structural criterion is not the onset of connectivity percolation but rather the percolation of particles with at least three bonds. This is a significant difference since the latter typically occurs at much later times, due to

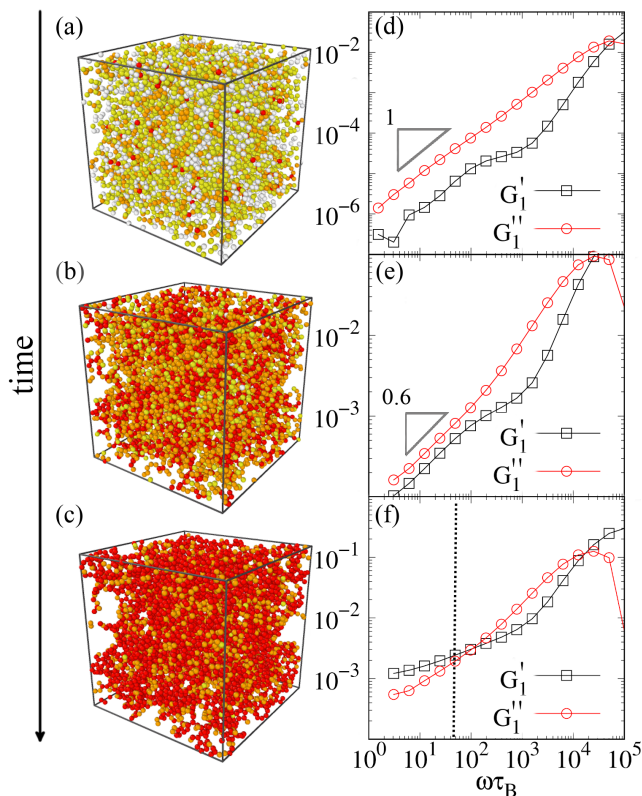


**FIG. 1. Time-dependence of the mechanical properties of a gel of spherical particles with valence three.** (a)-(c) three snapshots at different times. The color of each particle indicates its number of bonds: white (0), yellow (1), orange (2), and red (3). (d)-(f) the storage ( $G'_1$ ) and loss ( $G''_1$ ) moduli at the same times. (a) and (d) correspond to a viscoelastic fluid, (b) and (e) to a soft glassy material, and (c) and (f) to an elastic gel. Mechanical properties were measured in one sample of a cubic box of linear size  $L = 32$ , in units of the particle diameter, and number density  $\rho = 0.2$ .

the slow aging of the gel [13, 38, 63, 64]. Specific local geometric motifs, which may depend on the particle interactions, contribute to attaining rigidity, however it is their spatial organization and the way they are embedded in the structure that drives the onset of rigidity. Our results are consistent with, and provide further insight into, recent studies of nanoparticle gel rigidity [38, 65].

*Model.* We consider a monodisperse suspension of spherical colloidal particles of radius  $R$ . The valence of each particle is limited by adding pointlike attractive sites on the surface of the particles and considering that bonds are only established through the attractive sites. Thus, the number of attractive sites sets the valence. The pairwise interaction is then a superposition of an isotropic repulsion and a site-site attraction. As in previous works [63, 66], the repulsive interaction is given by,

$$U_{\text{colloid/colloid}}(r) = Ae^{-(r-2R)/k}, \quad (1)$$

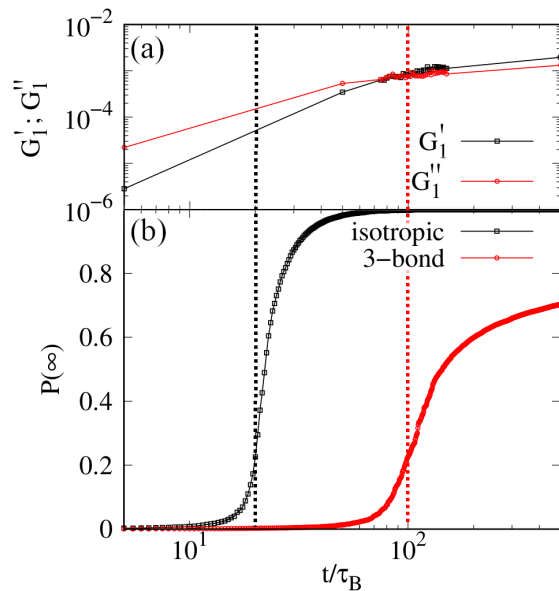


**FIG. 2. Mechanical and percolation properties of a gel of spherical particles with valence three.** (a) Storage  $G'_1$  and loss  $G''_1$  moduli as a function of time, measured at a frequency corresponding to the vertical line in Fig.1(f). (b) Fraction of particles,  $P(\infty)$ , in the largest connected component (black) and largest cluster of particles with three bonds (red) as a function of time. Vertical black (left) and red (right) dashed lines indicate the threshold for the connectivity and three-bond percolation transitions, respectively. All simulations were performed on a cubic box of linear size  $L = 32$ , in units of the particle diameter, number density  $\rho = 0.2$ , and the results are averaged over 10 samples for the percolation analysis and correspond to only one sample for the mechanical properties.

where  $r$  is the distance between the center of the particles,  $A = 1$  provides the energy scale, and  $k = 4$  is the screening length in reduced units. The bonding interaction is given by an inverted Gaussian potential,

$$U_{\text{site/site}}(r_s) = -\epsilon e^{-(r_s/\sigma)^2}, \quad (2)$$

where  $r_s$  is the distance between the attractive sites,  $\epsilon = 20$  is the interaction strength, and  $\sigma = 0.1R$  the width of the Gaussian in reduced units. The trajectories were obtained numerically by Langevin dynamics, using the LAMMPS [67], for diffusion coefficients for the translation  $D_t$  and rotational  $D_r$  motion that are related by the Debye-Einstein relation  $D_r = \frac{3}{4R^2}D_t$  [68].

We first consider particles with three attractive sites on a cubic box of linear size  $L = 32$  in units of the particle diameter and periodic boundary conditions in all directions. To form an elastic gel, the number density is set to  $\rho = 0.2$  and the temperature is  $k_B T/\epsilon = 0.025$ . The dynamics evolves over a total time of  $10^4 \tau_B$ , where  $\tau_B = 4R^2/D_t$  is the Brownian time.

*Rheological measurements.* We minimize the energy by

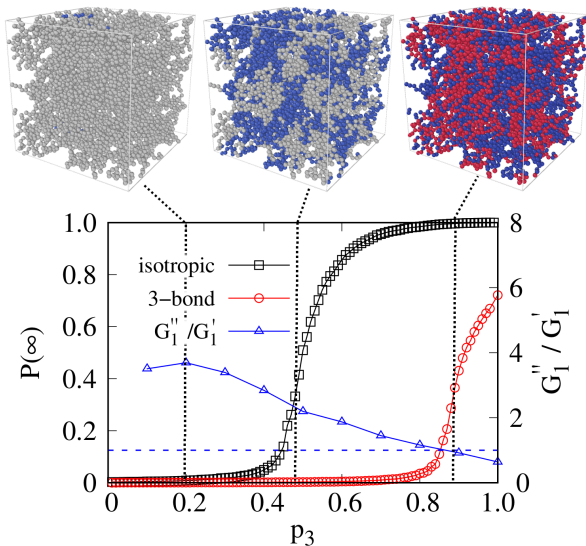


FIG. 3. **Percolation analysis of the mechanical properties of a gel of spherical particles with valence three, where sites are removed at random.** Fraction of particles,  $P(\infty)$ , in the largest connected component (black squares) and largest cluster of particles with three bonds (red squares) as a function of the fraction of the remaining particles with three attractive sites  $p_3$ . Loss factor (blue triangles)  $\tan(\delta) = G''_1/G'_1$  as a function of  $p_3$ . Top panel: Snapshots at three different stages (vertical dashed lines in the plot). Red particles are in the largest cluster of particles with three bonds (fully bonded), blue particles are in the largest connected component, and all the other particles are gray. All simulations were performed on a cubic box of linear size  $L = 32$ , in units of the particle diameter, for a number density  $\rho = 0.2$ . The results are averaged over 10 samples for the percolation analysis and correspond to only one sample for the mechanical properties.

running zero-temperature overdamped simulations until the kinetic energy is, at least ten orders of magnitude lower than its initial value [64]. Then, we apply Lees-Edwards boundary conditions and an affine shear deformation,

$$\mathbf{r}'_i = \begin{bmatrix} 1 & \gamma(t) & 0 \\ 0 & 1 & 0 \\ 0 & 0 & 1 \end{bmatrix} \mathbf{r}_i, \quad (3)$$

where  $\mathbf{r}_i$  and  $\mathbf{r}'_i$  are the initial and final positions of particle  $i$ , and  $\gamma(t)$  is the shear strain [64].  $\gamma(t)$  oscillates periodically in time,  $\gamma(t) = \gamma_0 \sin(\omega t)$ , with frequency  $\omega$  and amplitude  $\gamma_0$ . We computed the load curve to identify the linear regime. To focus on that regime, we set  $\gamma_0 = 0.07$ . The first-order storage  $G'_1$  and loss  $G''_1$  moduli are obtained from the time evolution of the shear stress  $\sigma_{xy}(t)$  as in Ref. [64].

Figures 1(a)-(c) are snapshots of the colloidal system at different times, where the color of a particle corresponds to the number of connected neighbors. Figures 1(d)-(f)

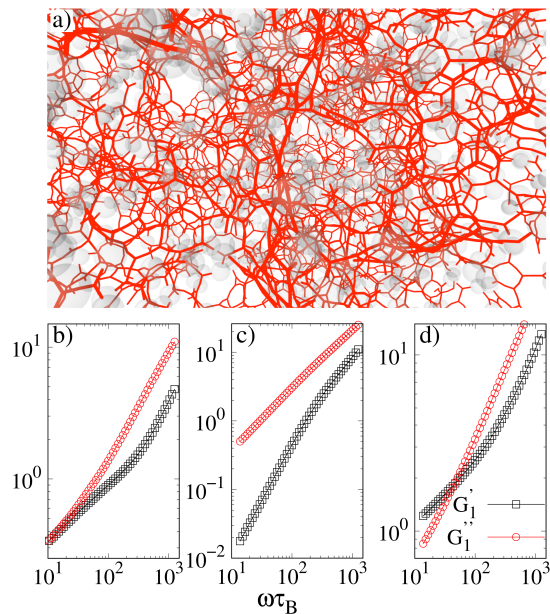


FIG. 4. **Structure and mechanical properties of the cluster of three-bonded particles.** (a) Snapshot of the largest connected component at the onset of rigidity, where the cluster of particles with three bonds is represented by the network of bonds (red) and all the other particles are in gray. (b), (c), and (d) are the storage  $G'_1$  and loss  $G''_1$  moduli as a function of the frequency  $\omega$ . (b) depicts the cluster of particles with three bonds (red network), (c) the largest connected component when we switch off the repulsive interactions during the rheological measurements, and (d) the largest connected component when we switch off the repulsive interaction only between the particles with less than three bonds during the rheological measurements. All simulations were performed on a cubic box of linear size  $L = 32$ , in units of particle diameter, and number density  $\rho = 0.2$ , for one sample.

show the  $\omega$  dependence of  $G'_1$  and  $G''_1$  for the three different regimes of gelation. Initially, in (a) and (d), most particles have established either one or no bonds.  $G'_1$  is lower than  $G''_1$  and it scales linearly with  $\omega$ , as in a Maxwell-like fluid [69]. As time evolves, more bonds are established and aggregates are formed with a characteristic size of several particles, affecting the mechanical response. For (b) and (e),  $G'_1$  is still lower than  $G''_1$  but both scale as  $\omega^\alpha$ , with  $\alpha < 1$ ; We estimate  $\alpha = 0.60 \pm 0.05$  [65]. Finally, in (c) and (f), a percolating network of particles with three bonds is already formed and the gel is rigid, since  $G'_1 > G''_1$  at low enough frequencies.

The time dependence of  $G'_1$  and  $G''_1$  for a frequency  $\approx 50 \tau_B^{-1}$  is shown in Fig. 2(a) (vertical line in Fig.1(f)). Both moduli increase with time and the transition to an elastic gel ( $G'_1 > G''_1$ ) occurs around  $100\tau_B$  (vertical red dashed line). The fraction of particles in the largest connected component is plotted in Fig. 2(b) (black curve). The onset of rigidity occurs much later than that for the

onset of connectivity percolation (vertical black dashed line, from Ref. [70]). However, if we compute the size of the largest cluster of fully-bonded particles (red curve), the data indicate that the onset of percolation of this subset coincides with the onset of rigidity.

To further test if the onset of rigidity coincides with the percolation threshold of particles with three bonds, we performed the following percolation analysis. We started from gel configurations at the final time of the simulations, when the gel is predominantly elastic and the particles with three bonds percolate. Then, at each iteration, one particle is selected and one of its attractive sites is removed. Both the particle and the attractive site are selected at random. We evaluate the mechanical and percolation properties as a function of  $p_3$ , defined as the fraction of particles that still have three attractive sites. Figure 3 depicts the dependence on  $p_3$  of the size of the largest connected component, the largest cluster of particles with three bonds and the ratio  $G'_1/G''_1$ . The data reveals that the onset of rigidity and the percolation of particles with three bonds coincide. Note that particles and attractive sites are selected uniformly at random, discarding possible effects from spatial correlations developed during the dynamics.

A snapshot of the largest connected component at the onset of rigidity is shown in Fig. 4(a), where the set of fully-bonded particles is represented by the network of bonds (red). The cluster of three-bonded particles forms a spanning network with cycles of at least five particles. Surprisingly, this structure is not rigid in itself, as shown in Fig. 4(b), where we plot  $G'_1$  and  $G''_1$  for that structure, when, during the rheological measurements, we neglect the interaction with all the other particles. Even when we consider the largest connected component (all particles), switching off the repulsive interactions between the particles, while keeping the bonding interaction, the structure is not rigid (see Fig. 4(c)). It is only when we include the repulsive interactions, at least between the particles with three bonds, that the structure becomes rigid (see Fig. 4(d)). Thus, although the onset of rigidity coincides with the percolation of particles with three bonds, it emerges from a combination of those bonds and repulsive (steric) interactions. These findings suggest that the rest of the structure in which the bond network is embedded contributes to rigidity.

*Effect of the valence.* So far, only particles of valence three have been considered. To evaluate the dependence on the valence, we performed the same percolation analysis for gels of particles with valence  $ns$  up to twelve, which is the number of neighbors in compact 3D packings. We select particles at random and remove all of their attractive sites but two. Thus, at each iteration the particles have either  $ns$  or two attractive sites. In Fig. 5, the size of the largest connected component (black) and the largest cluster of particles with at least three bonds (red) are plotted as a function of the fraction  $p_{ns}$  of par-

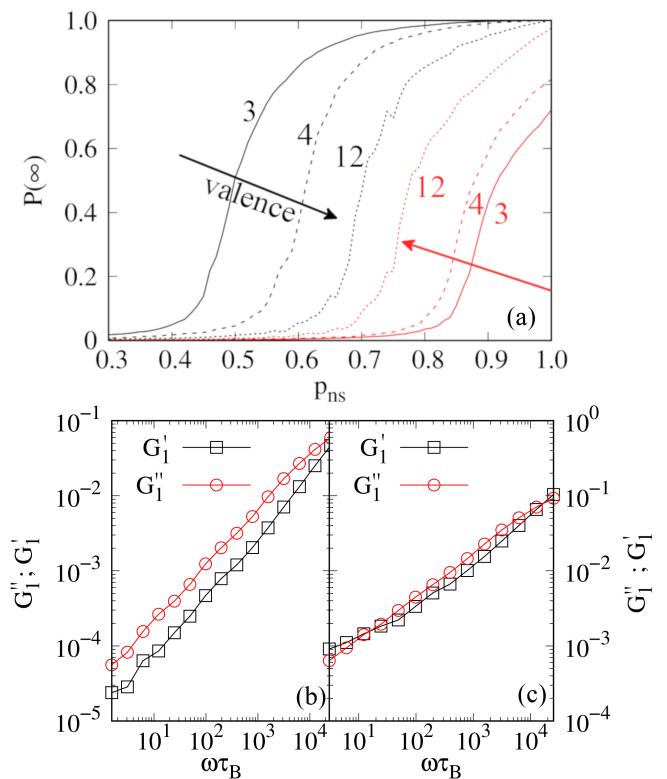


FIG. 5. **Dependence on the valence.** (a) Fraction of particles,  $P(\infty)$ , in the largest connected component (black) and largest cluster of particles with at least three bonds (red) as a function of the fraction of particles with  $ns$  attractive sites  $p_{ns}$ , where  $ns$  is the valence. Different curves are for different values of  $ns$ , namely, three (solid), four (dashed), and twelve (dotted). (b) and (c) Storage  $G'_1$  and loss  $G''_1$  moduli as a function of the frequency  $\omega$  for a fraction of particles with twelve attractive sites (b)  $p_{12} = 0.6$  and (c)  $p_{12} = 0.8$ , which are below and above the onset of percolation for particles with at least three bonds (see red dotted curve in (a)). All simulations were performed on a cubic box of linear size  $L = 32$ , in units of particle diameter, number density  $\rho = 0.2$ , and the results are averaged over 10 samples in (a) and are for one sample in (b) and (c).

ticles with  $ns$  attractive sites. The onset of the two percolation transitions depends strongly on the valence  $ns$ . While the one for connectivity percolation increases with  $ns$ , that for particles with at least three bonds shifts to lower values of  $p_{ns}$ . Thus, for particles with higher valence the two transitions are very difficult to distinguish experimentally.

Figure 5 also shows  $G'_1$  and  $G''_1$  as a function of  $\omega$  for a gel where  $ns = 12$ . We consider two different configurations (b)  $p_{12} = 0.6$  and (c)  $p_{12} = 0.8$ , which are below and above the onset of percolation for particles with at least three bonds. As in the case of  $ns = 3$  (Fig. 3), the  $G'_1$  is only larger than  $G''_1$  above the percolation transition for particles with at least three bonds. Below this

transition,  $G_1''$  is larger, over the entire range of frequencies, and thus the gel is not elastic but rather behaves as a viscous fluid.

*Conclusion.* We found that it is the combination of a bond network and repulsive contacts that leads to the rigidity of the gel. The development of rigid structures depends strongly on the gelation dynamics, not just on the number of bonds of a particle, as proposed by correlated rigidity percolation [13]. For all the gels considered here, where the particle valence ranged from three to twelve, we found that the onset of gel rigidity corresponds to the percolation of particles with at least three bonds, suggesting that for the type of interactions considered, this identifies the necessary condition for rigidity percolation. For nanoparticles with ad-hoc limited valence, our results provide the insight that a sufficient fraction of particles with valence three is required to design rigid structures. More generally, when the valence can not be controlled precisely, our findings shed light into how the mechanics of colloidal gels results from the interplay of different substructures intertwined with each other, not easily recognizable from local geometrical motifs.

*Acknowledgments.* We acknowledge financial support from the Portuguese Foundation for Science and Technology (FCT) under Contracts no. PTDC/FIS-MAC/28146/2017 (LISBOA-01-0145-FEDER-028146), PTDC/FIS-MAC/5689/2020, EXPL/FIS-MAC/0406/2021, CEECIND/00586/2017, UIDB/00618/2020, and UIDP/00618/2020. EDG acknowledge financial support from NSF DMR-2026842 and ACS Petroleum Fund. The authors also thank Minaspi Bantawa for support with the rheological tests.

---

\* csdias@fc.ul.pt

† fc51402@alunos.fc.ul.pt

‡ mmgama@fc.ul.pt

§ emanuella.del.gado@georgetown.edu

¶ nmaraujo@fc.ul.pt

- [1] P. J. Lu, E. Zaccarelli, F. Ciulla, A. B. Schofield, F. Sciortino, and D. A. Weitz, *Nature* **453**, 499 (2008).
- [2] P. N. Pusey and W. van Megen, *Nature* **320**, 340 (1986).
- [3] D. Bonn, H. Tanaka, G. Wegdam, H. Kellay, and J. Meunier, *Europhys. Lett.* **45**, 52 (1998).
- [4] C. L. Klix, C. P. Royall, and H. Tanaka, *Phys. Rev. Lett.* **104**, 165702 (2010).
- [5] A. M. Puertas, M. Fuchs, and M. E. Cates, *Phys. Rev. Lett.* **88**, 098301 (2002).
- [6] C. Ferreiro-Córdova, E. Del Gado, G. Foffi, and M. Bouzid, *Soft Matt.* **16**, 4414 (2020).
- [7] S. Griffiths, F. Turci, and C. P. Royall, *J. Chem. Phys.* **146**, 014905 (2017).
- [8] J. Colombo, A. Widmer-Cooper, and E. Del Gado, *Phys. Rev. Lett.* **110**, 198301 (2013).
- [9] S. Machlus, S. Zhang, and X. Mao, *Phys. Rev. E* **103**, 012104 (2021).
- [10] J. H. Cho, R. Cerbino, and I. Bischofberger, *Phys. Rev. Lett.* **124**, 088005 (2020).
- [11] J. M. Tavares, C. S. Dias, N. A. M. Araújo, and M. M. Telo da Gama, *J. Phys. Chem. B* **122**, 3514 (2018).
- [12] F. Bonacci, X. Chateau, E. M. Furst, J. Fusier, J. Goyon, and A. Lemaître, *Nat. Mater.* **19**, 775 (2020).
- [13] S. Zhang, L. Zhang, M. Bouzid, D. Z. Rocklin, E. Del Gado, and X. Mao, *Phys. Rev. Lett.* **123**, 058001 (2019).
- [14] J. Colombo and E. Del Gado, *Soft Matt.* **10**, 4003 (2014).
- [15] H. Tsurusawa, S. Arai, and H. Tanaka, *Sci. Adv.* **6**, eabb8107 (2020).
- [16] S. Mitura, A. Sionkowska, and A. Jaiswal, *J. Mater. Sci.: Mater. Med.* **31**, 50 (2020).
- [17] K. Ioannidou, M. Kanduč, L. Li, D. Frenkel, J. Dobnikar, and E. Del Gado, *Nat. Commun.* **7**, 12106 (2016).
- [18] S. Banerjee and S. Bhattacharya, *Crit. Rev. Food Sci. Nut.* **52**, 334 (2012).
- [19] I. Coropceanu, E. M. Janke, J. Portner, D. Haubold, T. D. Nguyen, A. Das, C. P. N. Tanner, J. K. Utterback, S. W. Teitelbaum, M. H. Hudson, N. A. Sarma, A. M. Hinkle, C. J. Tassone, A. Eychmüller, D. T. Limmer, M. Olvera de la Cruz, N. S. Ginsberg, and D. V. Talapin, *Science* **375**, 1422 (2022), <https://www.science.org/doi/pdf/10.1126/science.abm6753>.
- [20] C. S. Dias, C. A. Custodio, G. C. Antunes, M. M. Telo da Gama, J. F. Mano, and N. A. Araujo, *ACS Appl. Mater. Interfaces* **12**, 48321 (2020).
- [21] B. Ruzicka, E. Zaccarelli, L. Zulian, R. Angelini, M. Sztucki, A. Moussaïd, T. Narayanan, and F. Sciortino, *Nature Mater.* **10**, 56 (2010).
- [22] E. Bianchi, J. Largo, P. Tartaglia, E. Zaccarelli, and F. Sciortino, *Phys. Rev. Lett.* **97**, 168301 (2006).
- [23] F. Smallenburg and F. Sciortino, *Nature Phys.* **9**, 554 (2013).
- [24] A. B. Pawar and I. Kretzschmar, *Macromol. Rapid Commun.* **31**, 150 (2010).
- [25] K. J. Lee, J. Yoon, and J. Lahann, *Curr. Op. Coll. Interf. Sci.* **16**, 195 (2011).
- [26] Z. He and I. Kretzschmar, *Langmuir* **28**, 9915 (2012).
- [27] Y. Wang, Y. Wang, X. Zheng, É. Ducrot, J. S. Yodh, M. Weck, and D. J. Pine, *Nat. Commun.* **6**, 7253 (2015).
- [28] A. A. Shah, B. Schultz, K. L. Kohlstedt, S. C. Glotzer, and M. J. Solomon, *Langmuir* **29**, 4688 (2013).
- [29] E. Bianchi, B. Capone, G. Kahl, and C. N. Likos, *Faraday Discuss.* **181**, 123 (2015).
- [30] F. Romano, E. Sanz, and F. Sciortino, *J. Chem. Phys.* **134**, 174502 (2011).
- [31] O. Markova, J. Alberts, E. Munro, and P.-F. Lenne, *Phys. Rev. E* **90**, 022301 (2014).
- [32] D. Ortiz, K. L. Kohlstedt, T. D. Nguyen, and S. C. Glotzer, *Soft Matt.* **10**, 3541 (2014).
- [33] J. R. Wolters, G. Avvisati, F. Hagemans, T. Vissers, D. J. Kraft, M. Dijkstra, and W. K. Kegel, *Soft Matt.* **11**, 1067 (2015).
- [34] F. Smallenburg, L. Leibler, and F. Sciortino, *Phys. Rev. Lett.* **111**, 188002 (2013).
- [35] Q. L. Lei, X. Xia, J. Yang, M. P. Ciamarra, and R. Ni, *Proc. Natl. Acad. Sci. U.S.A.* **117**, 27111 (2020).
- [36] M. Capelot, M. M. Unterlass, F. Tournilhac, and L. Leibler, *ACS Macro Lett.* **1**, 789 (2012).
- [37] M. Liu, X. Zheng, V. Grebe, D. J. Pine, and M. Weck, *Nat. Mater.* **19**, 1354 (2020).
- [38] S. M. Fenton, P. Padmanabhan, B. K. Ryu, T. T. D. Nguyen, R. N. Zia, and M. E. Helgeson, *Proc. Natl.*

- Acad. Sci. U.S.A. **120**, e221592210 (2023).
- [39] P. J. Lu, E. Zaccarelli, F. Ciulla, A. B. Schofield, F. Sciortino, and D. A. Weitz, *Nature* **453**, 499 (2008).
- [40] M. Kohl, R. F. Capellmann, M. Laurati, S. U. Egelhaaf, and M. Schmiedeberg, *Nat. Commun.* **7**, 11817 (2016).
- [41] N. E. Valadez-Pérez, Y. Liu, A. P. R. Eberle, N. J. Wagner, and R. Castañeda-Priego, *Phys. Rev. E* **88**, 060302(R) (2013).
- [42] J. J. Richards, J. B. Hipp, J. K. Riley, N. J. Wagner, and P. D. Butler, *Langmuir* **33**, 12260 (2017).
- [43] C. I. N. Sampaio Filho, J. S. Andrade Jr., H. J. Herrmann, and A. A. Moreira, *Phys. Rev. Lett.* **120**, 175701 (2018).
- [44] D. J. Jacobs and M. F. Thorpe, *Phys. Rev. Lett.* **75**, 4051 (1995).
- [45] W. G. Ellenbroek, V. F. Hagh, A. Kumar, M. F. Thorpe, and M. van Hecke, *Phys. Rev. Lett.* **114**, 135501 (2015), 1412.0273.
- [46] E. Berthier, J. E. Kollmer, S. E. Henkes, K. Liu, J. M. Schwarz, and K. E. Daniels, *Phys. Rev. Mater.* **3**, 075602 (2019), 1812.07466.
- [47] H. Tsurusawa, M. Leocmach, J. Russo, and H. Tanaka, *Sci. Adv.* **5**, eaav6090 (2019).
- [48] R. Blumenfeld, S. F. Edwards, and R. C. Ball, *J. Phys. : Condens. Matter* **17**, S2481 (2005).
- [49] L. Feng, R. Dreyfus, R. Sha, N. C. Seeman, and P. M. Chaikin, *Adv. Mater.* **25**, 2779 (2013).
- [50] S. Sacanna, M. Korpics, K. Rodriguez, L. Colón-Meléndez, S.-H. Kim, D. J. Pine, and G.-R. Yi, *Nat. Commun.* **4**, 1688 (2013).
- [51] Y. Wang, D. R. Breed, V. N. Manoharan, L. Feng, A. D. Hollingsworth, M. Weck, and D. J. Pine, *Nature* **491**, 51 (2012).
- [52] M. Bantawa, W. A. Fontaine-Seiler, P. D. Olmsted, and E. Del Gado, *J. Phys. : Condens. Matter* **33**, 414001 (2021).
- [53] B. van der Meer, T. Yanagishima, and R. P. A. Dullens, **1**, 1 (2022), arXiv:2209.12703.
- [54] J. Russo, P. Tartaglia, and F. Sciortino, *J. Chem. Phys.* **131**, 014504 (2009).
- [55] N. A. M. Araújo, C. S. Dias, and M. M. Telo da Gama, *J. Phys.: Condens. Matter* **29**, 014001 (2017).
- [56] D. de las Heras, J. M. Tavares, and M. M. Telo da Gama, *Soft Matt.* **8**, 1785 (2012).
- [57] J. Russo, J. M. Tavares, P. I. C. Teixeira, M. M. Telo da Gama, and F. Sciortino, *Phys. Rev. Lett.* **106**, 085703 (2011).
- [58] J. Russo, F. Leoni, F. Martelli, and F. Sciortino, *Rep. Prog. Phys.* **85** (2022).
- [59] M. P. Howard, R. B. Jadrich, B. A. Lindquist, F. Khabaz, R. T. Bonnecaze, D. J. Milliron, and T. M. Truskett, *J. Chem. Phys.* **151**, 124901 (2019).
- [60] E. Zaccarelli, S. V. Buldyrev, E. La Nave, A. J. Moreno, I. Saika-Voivod, F. Sciortino, and P. Tartaglia, *Phys. Rev. Lett.* **94**, 218301 (2005).
- [61] E. Zaccarelli, I. Saika-Voivod, S. V. Buldyrev, A. J. Moreno, P. Tartaglia, and F. Sciortino, *J. Chem. Phys.* **124**, 124908 (2006).
- [62] E. Bianchi, R. Blaak, and C. N. Likos, *Phys. Chem. Chem. Phys.* **13**, 6397 (2011).
- [63] C. S. Dias, J. M. Tavares, N. A. M. Araújo, and M. M. Telo da Gama, *Soft Matt.* **14**, 2744 (2018).
- [64] J. Colombo and E. Del Gado, *J. Rheol.* **58**, 1089 (2014).
- [65] M. Bantawa, B. Keshavarz, M. Geri, M. Bouzid, T. Divoux, G. H. McKinley, and E. Del Gado, *Nature Physics* (2023), 10.1038/s41567-023-01988-7.
- [66] C. S. Dias, C. Braga, N. A. M. Araújo, and M. M. Telo da Gama, *Soft Matt.* **12**, 1550 (2016).
- [67] S. Plimpton, *J. Comp. Phys.* **117**, 1 (1995).
- [68] M. G. Mazza, N. Giovambattista, H. E. Stanley, and F. W. Starr, *Phys. Rev. E* **76**, 031203 (2007).
- [69] T. G. Mason and D. A. Weitz, *Phys. Rev. Lett.* **74**, 1250 (1995).
- [70] C. S. Dias, N. A. M. Araújo, and M. M. Telo da Gama, *J. Phys.: Condens. Matter* **30**, 014001 (2018).